A Monomeric, Biologically Active, Full-Length Human Apolipoprotein E[†]

Yonghong Zhang,[‡,§] Sheeja Vasudevan,[§,||] Radiya Sojitrawala,[||] Wentao Zhao,[‡] Chunxian Cui,[‡] Chao Xu,[||] Daping Fan,[||] Yvonne Newhouse,[⊥] Reeny Balestra,[⊥] W. Gray Jerome,[#] Karl Weisgraber,[⊥,▽,○] Qianqian Li,*[,‡] and Jianjun Wang*[,‡,||]

Department of Biochemistry and Molecular Biology, School of Medicine, Wayne State University, Detroit, Michigan 48201, Department of Biochemistry and Molecular Biology, School of Medicine, Southern Illinois University, Carbondale, Illinois 62901, Department of Pathology, Vanderbilt University Medical Center B-2101 MCN, 1161 21st Avenue, Nashville, Tennessee 37232-2561, Gladstone Institute of Neurological Disease, University of California, San Francisco, California 94158, and Department of Pathology and Cardiovascular Research Institute, University of California, San Francisco, California 94158

Received April 10, 2007; Revised Manuscript Received June 26, 2007

ABSTRACT: Apolipoprotein E (apoE) is an exchangeable apolipoprotein that plays an important role in lipid/lipoprotein metabolism and cardiovascular diseases. Recent evidence indicates that apoE is also critical in several other important biological processes, including Alzheimer's disease, cognitive function, immunoregulation, cell signaling, and infectious diseases. Although the X-ray crystal structure of the apoE N-terminal domain was solved in 1991, the structural study of full-length apoE is hindered by apoE's oligomerization property. Using protein-engineering techniques, we generated a monomeric, biologically active, full-length apoE. Cross-linking experiments indicate that this mutant is nearly 95−100% monomeric even at 20 mg/mL. CD spectroscopy and guanidine hydrochloride denaturation demonstrate that the structure and stability of the monomeric mutant are identical to wild-type apoE. Monomeric and wild-type apoE display similar lipid-binding activities in dimyristoylphosphatidylcholine clearance assays and formation of reconstituted high-density lipoproteins. Furthermore, the monomeric and wild-type apoE proteins display an identical LDL receptor binding activity. Availability of this monomeric, biologically active, full-length apoE allows us to collect high quality NMR data for structural determination. Our initial NMR data of lipid-free apoE demonstrates that the N-terminal domain in the full-length apoE adopts a nearly identical structure as the isolated N-terminal domain, whereas the C-terminal domain appears to become more structured than the isolated C-terminal domain fragment, suggesting a weak domain−domain interaction. This interaction is confirmed by NMR examination of a segmental labeled apoE, in which the N-terminal domain is deuterated and the C-terminal domain is double-labeled. NMR titration experiments further suggest that the hinge region (residues 192−215) that connects apoE's N- and C-terminal domains may play an important role in mediating this domain−domain interaction.

Human apoE is a 299-residue plasma exchangeable apolipoprotein that functions to transport and deliver lipids from one tissue or cell type to another *via* its interaction with the cell surface receptors of the LDL[1] receptor superfamily (*1*, *2*). This high-affinity binding of apoE to the receptors targets apoE-containing lipoprotein particles for endocytosis and intracellular degradation (*1*−*3*). As a component of a subclass of high-density lipoproteins (HDL) (HDL with apoE), apoE influences both cholesterol efflux and influx, thus playing an important role in reverse cholesterol transport (*4*). ApoE also plays an important role in neurological diseases (*5*). ApoE is produced in abundance in the brain and serves as the principal lipid transport vehicle in cerebrospinal fluid. In the case of peripheral nerve injury, apoE is induced at high local concentrations and was suggested to play a key role in repair of the injured nerve (*5*).

[†] This work was supported by RO1 grants from NIH (HL74365 to J.W., AG20235 to K.W., and HL49148 to W.G.J.). S.V. is supported by a postdoctoral fellowship and C.X. and D.F. are supported by a predoctoral fellowship from the American Heart Association (AHA 0420098Z to S.V., AHA 0215285Z to C.X., and AHA 0110244Z to D.F.).

* To whom correspondence should be addressed. Dr. Qianqian Li, Dr. Jianjun Wang, Department of Biochemistry and Molecular Biology, School of Medicine, Wayne State University, Detroit, MI 48201. Tel: 313-577-8836. Fax: 313-577-8836. E-mail: qil@med.wayne.edu and jjwang@med.wayne.edu.

[‡] Wayne State University.

[§] These authors contributed equally.

[||] Southern Illinois University.

[⊥] Gladstone Institute of Neurological Disease, University of California.

[#] Vanderbilt University Medical Center.

[▽] Department of Pathology, University of California.

[○] Cardiovascular Research Institute, University of California.

[1] Abbreviations: Aβ4, β-amyloid peptides; apoE, apolipoprotein E; apoE-J5, the monomeric apoE mutant; apoE-WT, wild-type apoE; apoEC, the apoE C-terminal domain; apoEN, the apoE N-terminal domain; CD, circular dichroism; DMPC, dimyristoylphosphatidylcholine; DPPC, dipalmitoylphosphatidylcholine; DSS, 2,2-dimethyl-2-silapentane-5-sulfonate; EPR, electron paramagnetic resonance; FRET, fluorescence resonance energy transfer; HDL, high-density lipoprotein; LDL, low-density lipoprotein; LDLR, low-density lipoprotein receptor; LRP, LDL-receptor related protein; NMR, nuclear magnetic resonance; POPC, palmitoyloleoylphosphatidylcholine; TCEP, tris[2-carboxyethyl]-phosphine; VLDL, very-low-density lipoprotein.

10.1021/bi700672v CCC: $37.00
Published on Web 08/23/2007

Three major isoforms of apoE have been identified: ApoE3 has a cysteine at 112 and an arginine at 158, while apoE2 has cysteines and apoE4 has arginines at both positions (*6*, *7*). These differences result in profound functional differences. ApoE2 binds to the LDL receptor defectively and is associated with type III hyperlipoproteinemia (*8*). Although apoE4 binds normally to LDL receptors, it is associated with elevated plasma cholesterol levels and a modest increase in cardiovascular disease (*9*, *10*). ApoE4 is the major genetic risk factor for late onset familial and sporadic Alzheimer's disease, as well as other forms of neurodegenerative disease (*11*−*13*).

ApoE is a two-domain protein that contains a 22 kDa N-terminal domain (residues 1−191) and a 10 kDa C-terminal domain (residues 216−299), linked by a protease sensitive hinge region (*1*). Experimental evidence indicates that these two domains fold independently and have distinct functions. While the N-terminal domain is responsible for LDL-receptor binding, the C-terminal domain binds to lipoproteins with a high affinity (*1*). The N-terminal domain of apoE is monomeric and its X-ray crystal structure in the lipid free state reveals a globular up-and-down four-helix bundle (*14*). Lipid-free full-length apoE forms oligomers at a very low concentration, and the C-terminal domain is responsible for oligomerization (*1*). The oligiomerization property hinders structural studies of lipid-free apoE using either X-ray crystallography or NMR techniques. Recently, crystallization of apoE bound to dipalmitoylphosphatidylcholine (DPPC) has been reported and the apoE molecular envelope determined to a 10 Å resolution (*15*). Based on this work, a model of apoE on DPPC particles has been proposed, suggesting that each apoE molecule is folded into a helical hairpin with the binding region for the LDL receptor at its apex (*15*).

The hinge region (residues 192−215) is unstructured, and its role in maintaining apoE's structure and contribution to apoE functions is not known (*1*). Although apoE's two domains fold independently, domain−domain interactions are observed that are suggested to regulate apoE's biological functions (*1*). Using X-ray crystallography and site-directed mutagenesis, it was demonstrated that, in apoE4 with arginine at position 112, arginine 61 extends out from the four-helix bundle and forms a potential salt bridge with glutamic acid 255. In apoE2 and apoE3 with cysteine at 112, the arginine 61 is in a different position where it is predicted not to interact with glutamic acid 255 to the same extent as apoE4 (*16*−*18*). This salt bridge between the two domains in apoE4 was hypothesized to change the overall conformation of apoE4 for its known VLDL binding preference and association with disease (*19*, *20*); apoE2 and apoE3 do not display this domain interaction to the same extent as apoE4 and preferably bind to HDL (*17*). The spatial proximity of the two domains of apoE was probed using the fluorescence resonance energy transfer (FRET) and electron paramagnetic resonance spectroscopy (EPR) techniques and demonstrated that the two domains are closer in both lipid-free and phospholipid-bound apoE4 than in apoE3, supporting the concept of domain interaction (*21*). However, both the FRET and EPR data indicated that the C-terminal domain of apoE3 also showed a weak interaction with the N-terminal domain (*21*, *35*). Nevertheless, a high-resolution structure of the full-length apoE is required to further define the structural basis of the apoE domain−domain interaction.

We recently reported the generation of a monomeric, biologically active apoE C-terminal domain (*22*). Using the same mutations, we report here a full-length apoE3 mutant that is monomeric at high concentrations. Most importantly, this monomeric apoE3 maintains the same structure and stability as the wild-type apoE3 and displays equal lipid-binding and LDL-receptor-binding activities. With this monomeric, biologically active apoE3, high quality NMR data has been collected, providing the opportunity for NMR structural determination of this important protein. In the present study, we also prepared a segmental labeled apoE3, in which the N-terminal domain is deuterated and the C-terminal is $^{15}N/^{13}C$ double-labeled. The NMR data of this segmental labeled apoE3 demonstrates that the structure of N-terminal domain is unaffected by the presence of the C-terminal domain, whereas the C-terminal domain in the intact protein adopts a more defined structure than it does as an isolated C-terminal domain fragment. This observation provides the NMR confirmation of domain−domain interaction in lipid-free apoE and the effect of the N-terminal domain on the C-terminal structure. NMR titration experiments further suggest that the hinge region between residues 192−215 may play an important role in positioning the domains for interaction.

MATERIALS AND METHODS

High-Level Expressions of Human ApoE. Two expression vectors were used to subclone apoE. One is an engineered pET30a(+) vector (Novagen) in which the long his-tag was replaced by a short his-tag (eight histidines), and the other is a pTYB vector (New England BioLab) with an intein fusion protein at the apoE C-terminus. The expressions were carried out using *Escherichia coli* BL-21(DE3) cells, similar to the apoE C-terminal domain (*22*). The purification procedures essentially follow the manuals. Using these expression vectors, we can routinely produce ∼20−60 mg/L of purified apoE. Isotope-labeling of apoE was achieved by expressing the protein in minimum medium made with 99% D_2O, in which NH_4Cl was replaced by $^{15}NH_4Cl$ or/and glucose was replaced by ^{13}C-glucose-C_6. Using several auxotrophic bacterial strains, we also prepared several specific ^{15}N-amino acid labeled apoE, such as ^{15}N-Arg apoE-(1−183) (*23*). Mass spectroscopy confirmed the correct molecular weight of apoE.

Site-Directed Mutagenesis. Site-directed mutagenesis was carried out using the QuickChange mutagenesis kit (Stratagene, CA). The mutations were confirmed by DNA sequencing.

Cross-Linking Experiments. ApoE (5−20 mg/mL) in 50 mM phosphate buffer, pH 7.5 was treated with 5 mM DTT overnight at 4 °C and then incubated for 30 min with bis-(sulfosuccinimidyl)suberate (BS_3, Pierce, final concentration 0.5 mM). The cross-linking reaction mixture was quenched by adding 1.0 M Tris-HCl and 5 X SDS−PAGE sample buffer, and then loaded on a 4−14% gradient SDS−PAGE gel.

DMPC Clearance Assay. 10 mg of DMPC (Avanti, AL) was dissolved in a mixture of chloroform and methanol (3:1 v/v) and dried using nitrogen gas and placed under vacuum for several hours. Prewarmed buffer (1 mL contain-

ing 10 mM Tris-HCl, pH 7.2, 150 mM NaCl, 0.5 mM EDTA) was added to make a final lipid concentration of 10 mg/mL and vortexed several times. Using a 200 nm filter, unilamellar vesicles were prepared by extrusion (*24*). Vesicles (100 μg) and apoE (100 μg) in buffer were added into a thermostated 1 mL cuvette and mixed for 5−10 s at 24 °C, and clearance of the solution was monitored using a Perkin-Elmer spectrophotometer (model Lambda 3B) at 490 nm as a function of time (*25*). All solutions were preincubated at 24 °C before the reaction.

Preparation of Reconstituted Discoidal HDL. The rHDL particles were prepared using the sodium cholate dialysis method (*26*, *27*) with palmitoyloleoylphosphatidylcholine (POPC), apoE, and sodium cholate in a molar ratio of 100:1:135. POPC was dissolved in $CHCl_3$ and dried under nitrogen, then resuspended in Tris buffer, and vortexed thoroughly. Sodium cholate was added into the POPC solution, and the mixture was vortexed again for another 3 min. The dispersion was incubated at 37 °C and vortexed every 15 min until completely clear. ApoE was added, and the mixture was incubated for 1 h at 37 °C. The sodium cholate was removed by exhaustive dialysis.

LDL Receptor Binding Assay. ApoE proteins were complexed with DMPC and isolated by KBr gradient centrifugation (*28*). The apoE·DMPC complexes were characterized using electron microscopy, and it was found that the complexes formed by the monomeric apoE3 were the same size as wild-type apoE3. The receptor binding activities of the apoE·DMPC complexes were determined in a competition assay with ^{125}I-labeled human LDL and human primary fibroblasts in culture, as previously described (*28*).

Electron Microscopy. The apoE·DMPC complexes and rHDL were sized using negative staining electron microscopy. The particles were adsorbed to hydrophilic, carbon, and Formvar-coated grids. Samples were negatively stained for 20 s with 2% phosphotungstic acid, pH 6.7. Digital images were taken using a Philips CM-12 electron microscope operated at 80 keV accelerating voltage. At least 10 arbitrarily selected fields were chosen for measurement (>200 particles per condition).

CD Spectroscopy and Stability Measurement. CD measurements were carried out on an AVIV model 62DS CD spectrometer (AVIV). The secondary structure contents of apoE and mutants were calculated from CD data based on Morrow et al. (*36*). For chemical denaturation, data was collected at a single wavelength for 100 s using time constants of 5 to 10 s. Guanidine hydrochloride denaturation was performed as described (*29*) and monitored by CD at 220 nm in a 0.1 cm cuvette. Individual 0.4 mL samples were prepared by weight for each denaturant concentration. The concentrations of protein and denaturant were determined using the density formulas given by Pace *et al.* (*29*).

Preparation of a Segmental Labeled ApoE. We developed an on-column ligation method to prepare segmental labeled apoE. Two DNA constructs, apoE(1−214)/pTYB1 and apoE-(C215−299)-J5/pET30a, were generated. In the apoE(C215−299)-J5/pET30a, we engineered the pET30a expression vector to include a Factor Xa cleavage site between the his-tag and apoE(C215−299)-J5. Bacterial expression produced two apoE domains: apoE(1−214)-intein-CBD and his-tag-apoE(C215−299)-J5. ApoE(1−214) was perdeuterated, and his-tag-apoE(C215−299)-J5 was double-labeled with ^{13}C/^{15}N. Factor Xa was used to remove the long his-tag from apoE(C215−299)-J5. However, we observed a nonspecific Factor Xa cleavage site at position of R217, which represented the major cleavage site. This nonspecific cleavage removed the N-terminal Cys of apoE(C215−299), making native chemical ligation impossible. To solve this problem, we prepared a R217S mutation of apoE(C215−299) that completely eliminated this nonspecific cleavage. We optimized the bacterial expression level of apoE(1−214)-intein-CBD, and these optimizations significantly enhanced the final yield of apoE(1−214)-intein-CBD. For apoE(1−214)/pTYB1 expression, glycerol stock was added into 300 mL of LB with 1 mM ampicillin. The expression grew at 37 °C until OD_{600} reached 2.5−3.0. The bacteria were gently spun down and transferred into 300 mL of M9 medium that contained 1% glucose, 1/100 x Vitamin, pH8.0. The expression was carried out at 20 °C for 1.5 h, and 0.5 mM IPTG was then added to induce protein expression. The protein expression was further carried out at 20 °C for another 22 h before harvesting the cells. We purified apoE(1−214)-intein-CBD based on the manual and left the purified apoE fusion protein bound to the column. We then added apoE(C215−299)-J5 at a 5:1 molar ratio between apoE(C215−299) and apoE-(1−214)-intein-CBD. A thiol reagent, thiol phenol, was also added for ligation in the presence of TCEP for 18−24 h at room temperature. The ligation product was purified using a heparin column, CL-6B. The purified segmental labeled apoE was dialyzed in water with 25 mM ammonium bicarbonate and then lyophilized. This on-column ligation method allows us to produce a large yield of segmental triple-labeled apoE-J5 (25−30 mg/L, ^{2}H-apoE(1−214)-^{13}C/^{15}N-apoE(C215−299)-J5). The details of this method will be published elsewhere.

NMR Methods. NMR samples contained 0.5−1.0 mM ^{2}H-(99%)/^{15}N/^{13}C-labeled apoE in 95%H_2O/5%D_2O, 25 mM phosphate buffer containing 25 mM NaCl (pH 6.9), 0.25 mM NaN_3, 10 mM DTT and 10 mM EDTA. The chemical shift was referenced using DSS at 0 ppm. All NMR experiments were performed at 30 °C on a VARIAN INOVA 600 spectrometer equipped with a triple-resonance, *z*-axis gradient cold probe. The 2D ^{1}H−^{15}N HSQC collected was a sensitivity-enhanced experiment with 1024 points at the proton dimension and 256 complex points at the ^{15}N dimension. The acquisition times for both dimensions were 64 ms. The NMR titration experiments were carried out and the spectral changes were monitored using 2D ^{1}H−^{15}N HSQC spectra. The NMR data processing was achieved using nmrPipe software (*30*).

RESULTS AND DISCUSSION

High-Level Expression of Human ApoE3. Using our expression vectors, we successfully produced high yields of apoE (20−60 mg/L) (Figure 1, panel A). The expressed his-tag apoE3 contains only eight histidines. For production of apoE3 without a tag, we used a pTYB vector, in which the intein fusion protein was placed at the C-terminus of apoE3. We noticed that the expression yield of the monomeric apoE3 (50−60 mg/L) is higher than that of the wild-type apoE3 (20−30 mg/L). Nevertheless, these two high-level expression vectors allowed us to produce sufficient amounts of apoE proteins for biophysical and biochemical characterization of this protein. More importantly, we were able to produce a

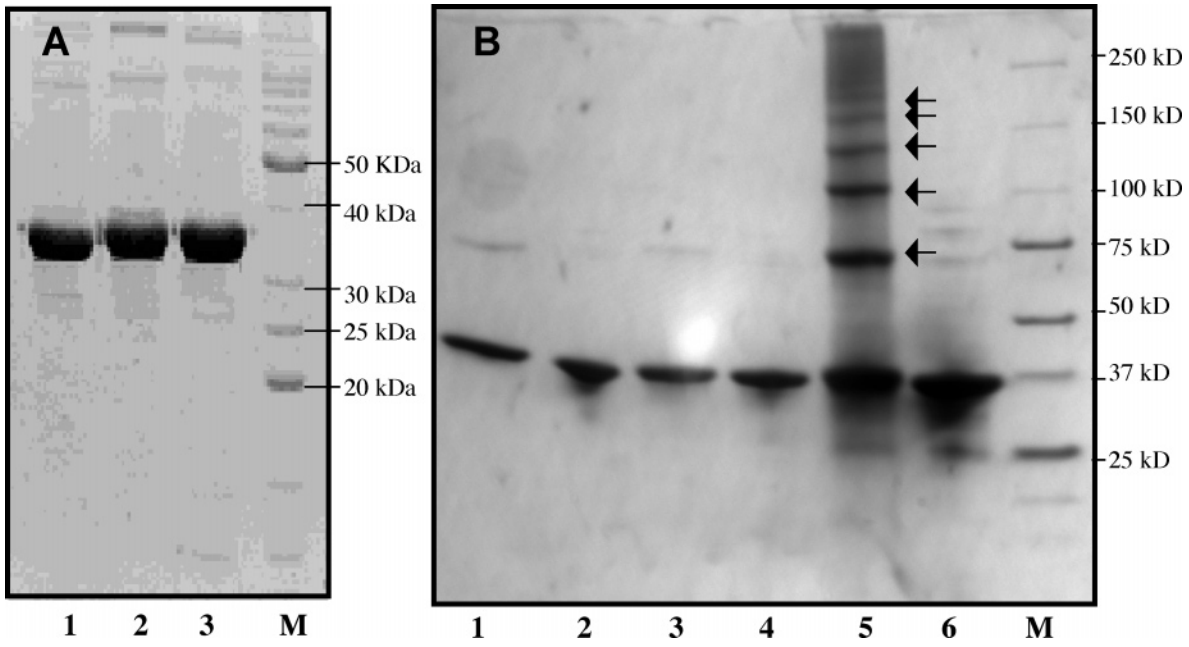

FIGURE 1: Panel A. A SDS−PAGE of the purified apoE3 and mutants. M. Bench marker. 1. ApoE3-WT. 2. ApoE3-J4. 3. ApoE3-J5. Panel B: A 4−14% gradient SDS−PAGE of cross-linking results of full-length apoE3. M. Bench Marker. 1. ApoE3-J4 mutant with cross-linker. 2. ApoE3-J4 mutant without cross-linker. 3. ApoE3-J5 mutant with cross-linker. 4. ApoE3-J5 mutant without cross-linker. 5. ApoE3-WT with cross-linker. 6. ApoE3-WT without cross-linker. Cross-linker: BS3. ApoE3-J4 and apoE3-J5: 20 mg/mL. ApoE3 wild-type: 5 mg/mL. Arrows: dimer, trimer, tetramer, and higher oligomers.

large amount of triple-labeled ($^{2}H/^{13}C/^{15}N$) apoE3, leading to a low cost NMR study of this protein.

A Monomeric, Full-Length ApoE3. Previously, we reported a monomeric apoE C-terminal domain that is biologically active (*22*). Using the same strategy, we also prepared a monomeric, biologically active mouse apoAI mutant (*31*). These successes encouraged us to attempt the preparation of a monomeric, full-length apoE that is biologically active. In addition, our NMR data on the isolated apoE N-terminal domain also suggested that this domain is monomeric even at 1 mM concentration (*32*). Using the same mutations, we prepared a full-length apoE3 mutant, apoE3-J5 (F257A/W264R/V269A/L279Q/V287E), and another mutant apoE3-J4, containing four mutations (F257A/W264R/L279Q/V287E). Cross-linking results (Figure 1, panel B**)** clearly demonstrate that while the wild-type apoE adopts a mixture of monomer (40%), dimer (20%), trimer (15%), tetramer (10%), and other higher oligomers (15%) at 5 mg/mL, apoE3-J4 and apoE3-J5 are predominantly monomeric (>95%) with a minor species of dimer (<5%) at 20 mg/mL. When comparing apoE3-J4 to apoE3-J5, no major difference was observed. The fact that the same mutations in the monomeric apoE C-terminal domain also result in a monomeric full-length apoE3 confirms that the C-terminal domain of apoE is responsible for apoE's oligiomerization. In addition, this data also demonstrates that the following four residues are critical for apoE's oligiomerization: F257, W264, L279, and V287. The remaining question is: Do the mutations of these four residues affect the structural and functional integrity of apoE?

The Monomeric ApoE Maintains ApoE's Structure and Stability. We next characterized the structure and stability of the monomeric apoE3 mutants and compared to wild-type apoE3. Far-UV CD spectra provide secondary structural information of a protein, and near-UV CD spectra identify the microenvironment of aromatic residues, providing tertiary structural information of a protein. The CD spectra clearly demonstrated that the monomeric apoE3 mutants, both apoE3-J4 and apoE3-J5, adopt an identical secondary and tertiary structure as the wild-type apoE3 (Figure 2, panel A). The far-UV CD spectra indicated that the helix content of the monomeric apoE mutants, including apoE-J4 (62%) and apoE-J5 (60%), is nearly identical to the wild-type apoE3 (61%). The minor spectral difference in the near UV region is due to the mutation of W264R in the apoE3-J5 mutant, however, the overall near UV CD spectra show a similar spectral curve, suggesting that the tertiary structure of apoE3 was not altered by the mutations in apoE3-J5. Using CD spectroscopy, GdnHCl denaturation comparisons were performed. As shown in Figure 2, panel B, the denaturation curves of the monomeric apoE3-J5 and apoE3-WT, indicate that both proteins have identical stabilities. The denaturation curves display transitions with midpoints at 0.9 and 2.5 M GdnHCl. Previously, it was demonstrated that these transitions represented the denaturation of the C- and N-terminal domains of apoE3, respectively (*33*). This is a characteristic property of apoE3, and the mutations in apoE3-J5 preserve this property. The identical transitions in the apoE3-J5 curve strongly indicate that it maintains the same tertiary structure and stability as the apoE3-WT.

To further confirm the structural integrity of monomeric, full-length apoE3, we triple-labeled apoE3-J5 and performed NMR analysis. Figure 3 shows $^{1}H-^{15}N$ HSQC spectra of the triple-labeled, monomeric apoE3 (panel A), an isolated apoE3 N-terminal domain fragment (panel B) and an isolated apoE C-terminal domain fragment (panel C). The spectral assignment of the apoE3 N-terminal domain is reported elsewhere (*32*). The data clearly demonstrates that apoE3-J5 produces a high quality spectrum that can be used for a complete spectral assignment. Indeed, a two-dimensional $^{1}H-^{1}H$ NOESY spectrum of 50% deuterated apoE3-J5 shows a large amount of NOEs, including many HN−HN NOEs

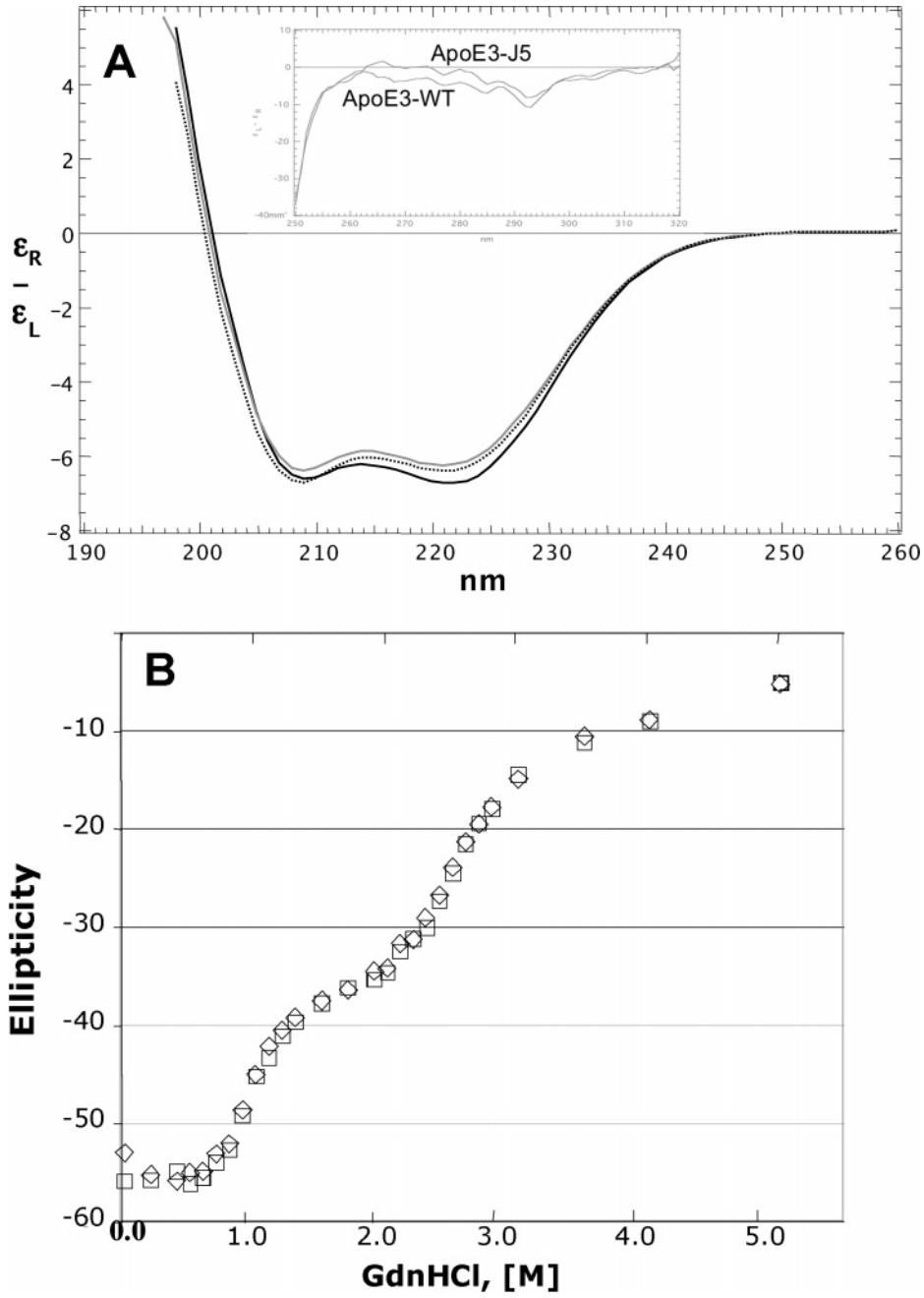

FIGURE 2: Panel A. Far-UV CD spectra of apoE3-WT (dotted), apoE3-J5 (gray), and apoE3-J4 (black). Inset: Near-UV CD spectra of apoE3-WT and apoE3-J5. Panel B. GdnHCl denaturation of apoE3-WT (diamond) and apoE3-J5 (square). Protein concentrations are 0.25 mg/mL. Both apoE3-WT and apoE3-J5 show two transitions in the denaturation curves.

(data not shown), suggesting the likelihood for a complete structural determination. Panel A also indicates that apoE3-J5 properly folds to adopt a well-defined helix-bundle structure, since the backbone amide proton chemical shift dispersion is about 3.2 ppm. In comparison with panel B, we observed that part of the spectral pattern of full-length apoE3-J5 is nearly identical to the pattern of the isolated apoE3 N-terminal domain, apoE3(1−183), especially for those well-dispersed cross-peaks. This suggests that the N-terminal domain structure does not undergo a significant structural change between an isolated apoE N-terminal domain and this domain in the full-length apoE3. Indeed, the identical cross-peak positions between panels A and B allow us to assign many cross-peaks in apoE3-J5. Since the apoE3(1−183) in panel B is a wild-type apoE N-terminal domain, the identical spectral pattern shown in panels A and B confirms that the monomeric apoE3-J5 maintains the structural integrity of apoE3-WT, at least in the N-terminal domain.

The Monomeric ApoE3-J5 Maintains Full Lipid-Binding Activity of ApoE3-WT. To examine if the monomeric apoE3-J5 is functional, we first tested its lipid-binding activity because it is essential for apoE's LDL receptor binding activity. Two lipid-binding assays were used: a DMPC clearance assay and formation of reconstituted discoidal HDL particles using the cholate dialysis method. The DMPC binding assay is widely used to characterize the lipid-binding activity of exchangeable apolipoproteins. To our surprise, the wild-type apoE3 displays a slower clearance rate than that of the two monomeric apoE3 mutants under the

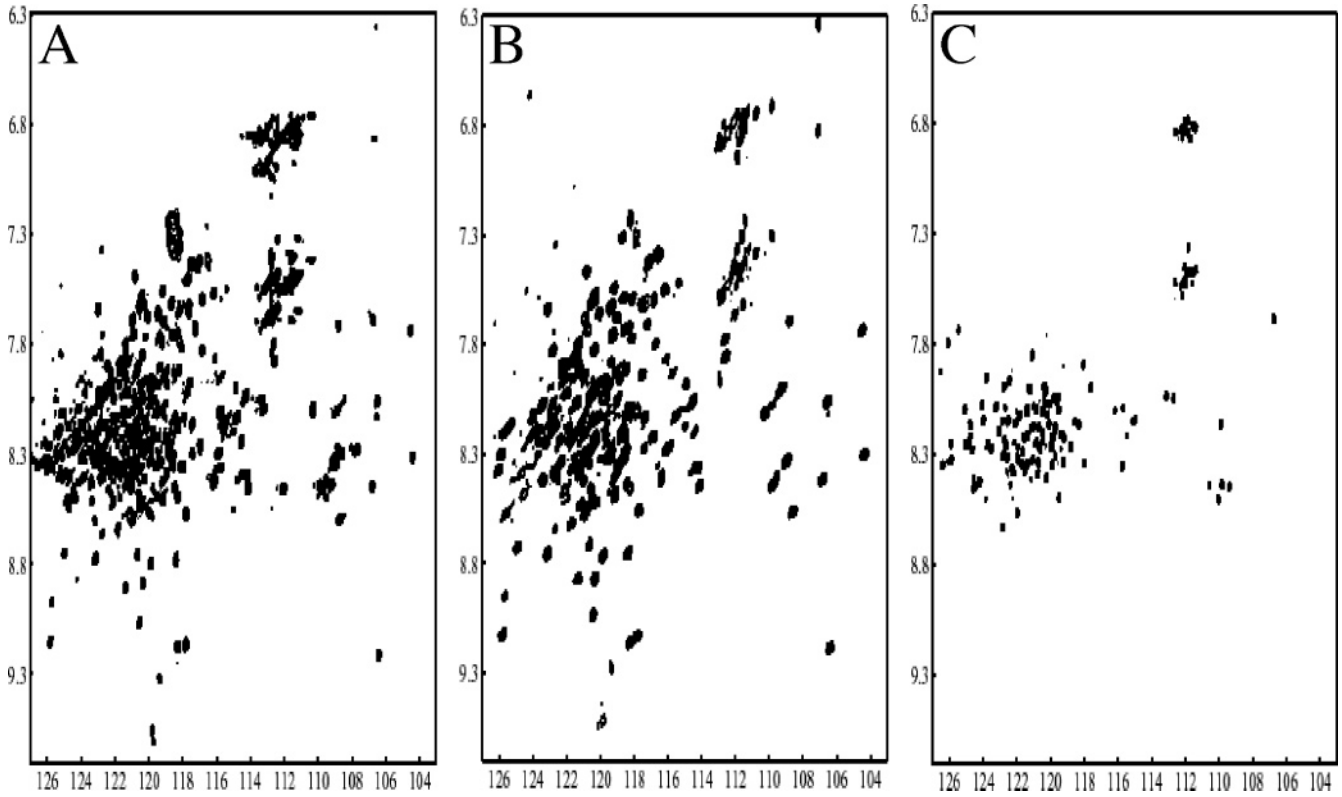

FIGURE 3: Panel A. $^{1}H-^{15}N$ HSQC spectrum of the monomeric apoE3-J5(1−299) in 25 mM phosphate buffer containing 25 mM NaCl, 10 mM EDTA, 10 mM DTT, pH 6.9. Panel B: $^{1}H-^{15}N$ HSQC spectrum of the monomeric apoE3(1−183) in 100 mM phosphate buffer containing 10 mM EDTA, 20 mM DTT, pH 6.8. Panel C: $^{1}H-^{15}N$ HSQC spectrum of the monomeric apoE3-J5(200−299) in 100 mM phosphate buffer, pH 6.8.

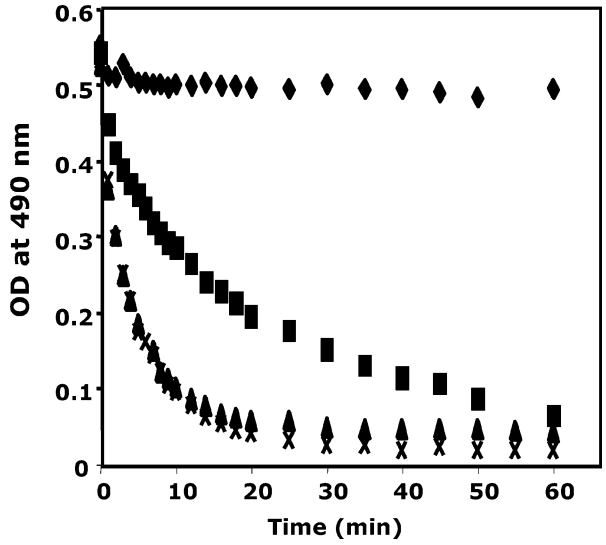

FIGURE 4: DMPC clearance assay. DMPC vesicles were incubated at 24 °C in the absence (◆) and presence of apoE3-WT (■), apoE3-J4 (▲) and apoE3-J5 (×) in 10 mM Tris-HCl, pH 7.2, 150 mM NaCl, 0.5 mM EDTA. Vesicle clearance as a function of time was followed by measuring OD at 490 nm.

conditions that were used (100 μg of DMPC/100 μg of protein, pH 7.2) (Figure 4). However, all three proteins display a nearly equal turbidity at 60 min, indicating that they share an equal ability of transforming large DMPC vesicles into smaller apoE3·DMPC particles. To confirm this result, we carried out this assay under different conditions (250 μg of DMPC/200 μg of apoE3, pH 6.5). The result confirmed the previous finding, indicating that the wild-type apoE3 indeed displayed a slower clearance rate than the monomeric mutants. The slower clearance rate by the wild-type apoE3 may be due to the oligomeric states of this protein. To transform large DMPC vesicles into smaller apoE3·DMPC particles, oligomeric wild-type apoE3 may have to go through a structural reorganization process to form discoidal particles. In contrast, the monomeric apoEs do not need to go through this process, thus displaying a faster clearance rate. To verify that the monomeric apoE3 proteins generate HDL particles with DMPC, we examined the final products of the DMPC assay on native gels. The data indicate that both apoE3-J5 and wild-type apoE3 generate HDL particles with no lipid-free and lipid-poor particles observed (Figure 5, panel D, inset). There were no size differences among the HDL particles generated using different apoE3 proteins. This is confirmed by negative staining electron microscopy (Figure 5, panels C and D). The apoE·DMPC particles show an average diameter of 11.5 ± 4.0 nm. Using a cholate dialysis method, we also prepared rHDL particles with POPC and characterized these rHDL using native gel and electron microscopy. Since apoE has an ability to prepare HDL particles *in vivo* (*34*), this assay is also often used to access apoE's lipid-binding activity. In addition, POPC is a physiological phospholipid, and this assay serves as an alternative assay of mimicking the *in vivo* lipid-binding activity of apoE. The native gel indicates no major difference between the rHDLs prepared with either apoE3-J5 or wild-type apoE3 (Figure 5, panel A, inset). These rHDLs have a homogeneous size of $\sim 10.5 \pm 2.5$ nm, and no lipid-poor or

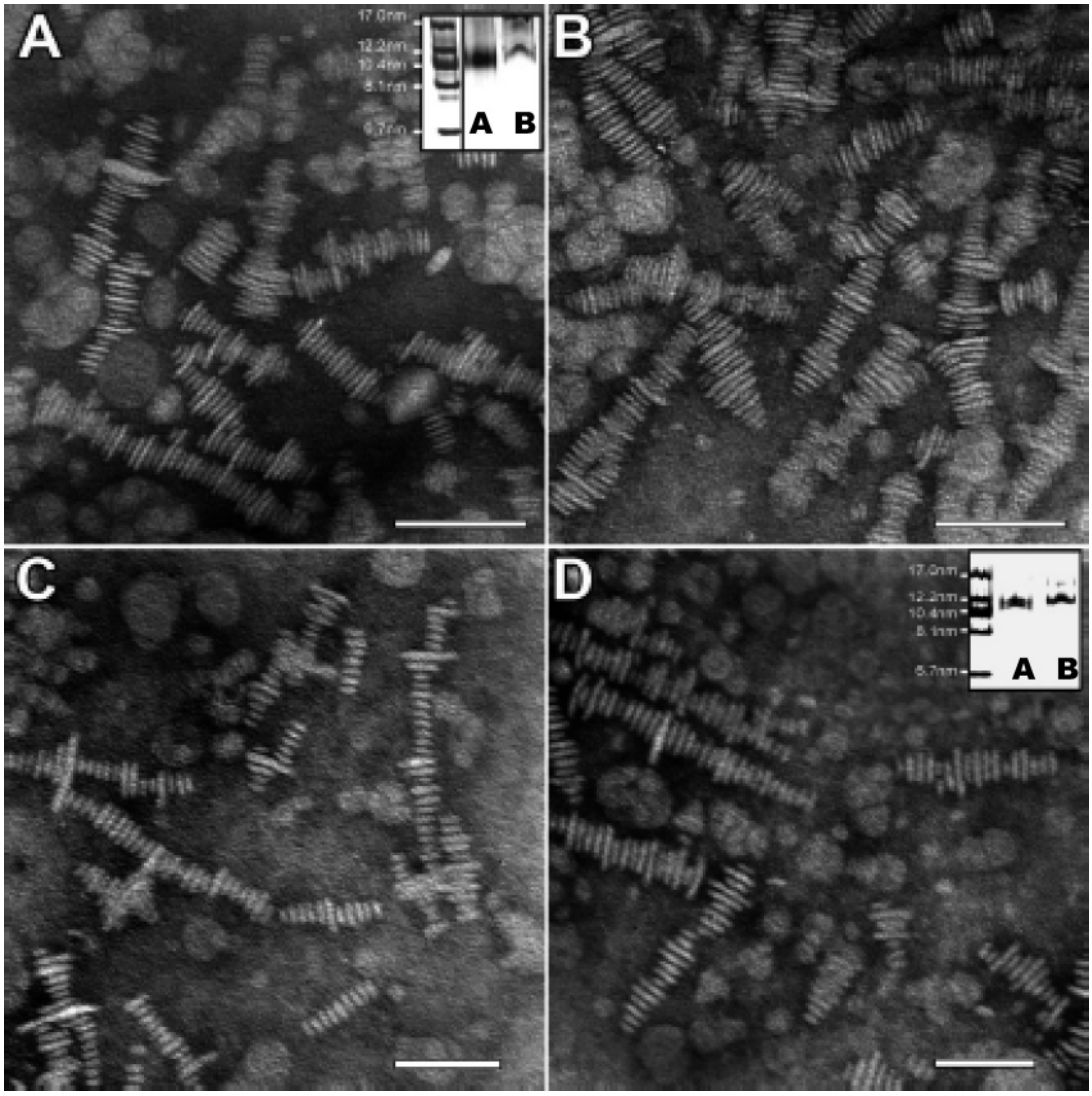

FIGURE 5: Electron microscopy and gel electrophoresis of the HDL particles prepared using apoE3 proteins with either POPC or DMPC. Panel A: Human apoE3-WT with POPC. Panel B: The monomeric apoE3-J5 with POPC. Panel C: Human apoE3-WT with DMPC. Panel D: The monomeric apoE3-J5 with DMPC. The white bars shown in panels A, B, C, and D are 50 nm. The inset in panel A is a 4−15% gradient native PAGE of the discoidal HDL particles prepared using apoE3-WT (lane A) and apoE3-J5 (lane B) with POPC. The inset in panel D is a 4−15% gradient native PAGE of the HDL particles prepared using apoE3-WT (lane A) and apoE3-J5 (lane B) with DMPC. The particle sizes of apoE/POPC are at a diameter of ∼10.5 ± 2.0 nm and apoE/DMPC are at a diameter of ∼11.5 ± 4.0 nm.

lipid-free apoE3 are observed. This result is also confirmed by electron microscopic data (Figure 5, panels A and B), suggesting an identical morphology and size of the rHDLs (10.5 nm). In addition, CD spectroscopic data indicated that both the wild-type apoE3 (72% helix) and the monomeric apoE3-J5 (73% helix) shared a nearly identical alpha-helical content on POPC particles. Based on the above results, we conclude that the monomeric apoE3-J5 maintains the lipid-binding activity of apoE3.

The Monomeric ApoE3-J5 Displays Full LDL-Receptor Binding Activity of ApoE3. Another important biological function of apoE is its LDL-receptor-binding activity. To examine if the monomeric apoE3-J5 binds to the LDL-receptor, we performed a LDL-receptor-binding assay. The results demonstrate that the monomeric apoE3 mutants/DMPC and wild-type apoE3/DMPC displayed an identical ability of competing with human ^{125}I-LDL for binding to the LDL receptor on normal human fibroblasts, suggesting that they share an identical binding activity to the LDL receptor (Figure 6).

Lipid-Free ApoE3 Displays a Weak Domain−Domain Interaction. Previous FRET/EPR data indicate that the C-terminal domain of apoE3 is also in a close proximity to the N-terminal domain (*21*). This raises a question about domain−domain interaction in apoE3. Does the close proximity of the two domains in apoE3 have a structural consequence? To answer this question, we performed two NMR studies of apoE3. In the first study, a segmental labeled full-length apoE3-J5, in which the N-terminal domain is deuterated whereas the C-terminal domain is ^{13}C/^{15}N double-labeled (^{2}H-apoE3(1−214)-^{13}C/^{15}N-(215−299)-J5), was examined. In the second study an isolated double-labeled apoE C-terminal domain (^{13}C/^{15}N-apoE3(215−299)-J5) was examined. The ^{15}N−^{1}H HSQC spectra for both samples were collected. The ^{15}N−^{1}H HSQC spectrum of a segmental labeled apoE is shown in Figure 7, panel A, and the spectrum

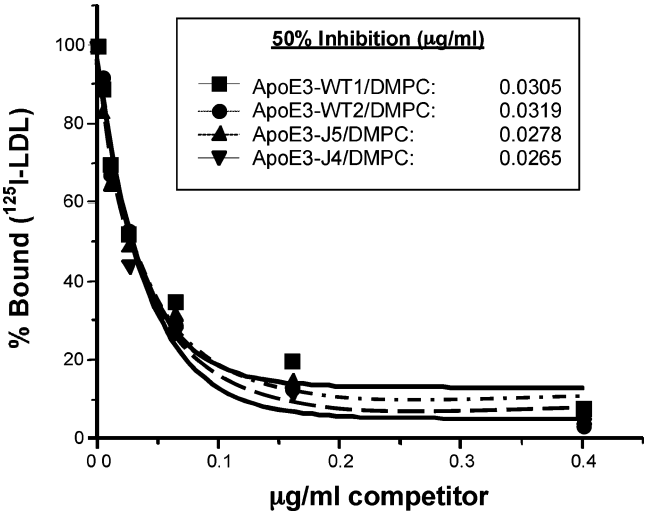

FIGURE 6: Plot showing the ability of apoE·DMPC particles to compete with human ^{125}I-LDL for binding to the LDL receptor on normal human fibroblasts. Two sources of apoE3 wild-type proteins are used in this experiment as controls: apoE3-WT1, the wild-type apoE3 generated from Wang's laboratory; apoE3-WT2, the wild-type apoE3 generated from Weisgraber's laboratory. Data presented are from four experiments. ■: ApoE3-WT1/DMPC. ●: ApoE3-WT2/DMPC. ▲: ApoE3-J5/DMPC. ▼: ApoE3-J4/DMPC.

of the isolated apoE C-terminal domain is shown in panel B. Since the N-terminal domain (^{2}H-apoE3(1−214)) of this segmental labeled apoE is deuterated, it is transparent in this spectrum. The NMR signals of panel A arise from the apoE C-terminal domain that is double-labeled with ^{15}N and ^{13}C.

A careful comparison between these two spectra in Figure 7 revealed several spectral differences. Although the chemical shift dispersion of the backbone amide proton of these two spectra is very similar, they display a different spectral pattern, highlighted by arrows and boxed regions, suggesting a potential structural difference between the isolated apoE C-terminal domain and this domain in the context of full-length apoE3. Extra cross-peaks in the isolated apoE C-terminal domain (shaded arrows in the boxed regions) suggest that this domain may display conformational heterogeneity in solution as an isolated fragment. However, this conformational heterogeneity disappears in the context of full-length apoE3. For example, apoE(215−299)-J5 contains 3 glycines. Panel A of Figure 7 only shows three Gly cross-peaks as highlighted by three shaded arrows in the right side of the boxed region. In contrast, the same region of panel B shows five Gly cross-peaks as highlighted by five shaded arrows in the right side of the boxed region. Similar heterogeneity cross-peaks are also observed for the other residues as highlighted by the other two shaded arrows in the boxed region (panel B). Interestingly, among three Gly residues in apoE(215−299)-J5, only two Gly residues show conformational heterogeneity (lower right four shaded arrows in the boxed region). The third Gly residue does not show any conformational heterogeneity (higher right shaded arrow in the boxed region). In addition, many more side chain cross-peaks of Asn and Gln are observed in the apoE C-terminal domain in the segmental-labeled apoE3 (cross-peaks linked by dotted lines in the upper right corner, panel A) than those in an isolated apoE C-terminal domain (cross-peaks linked by dotted lines in the upper right corner, panel B). In the apoE3(215−299)-J5, there are 10 Gln and 1 Asn

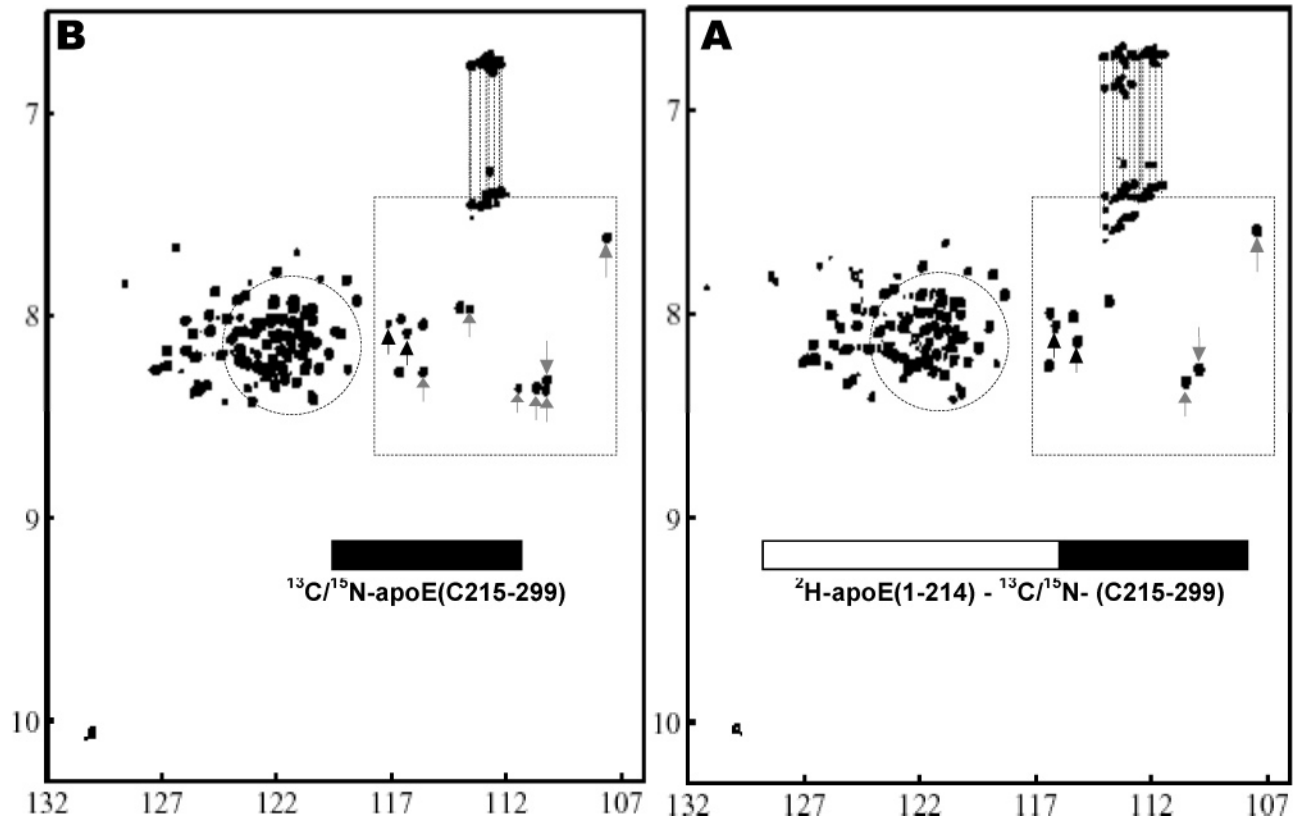

FIGURE 7: ^{1}H−^{15}N HSQC spectra of a segmental labeled apoE3, ^{2}H-apoE3(1−214)-^{13}C/^{15}N-apoE-J5(215−299) (panel A), and an isolated ^{13}C/^{15}N apoE-J5(215−299) (panel B), in 25 mM phosphate buffer containing 25 mM NaCl, 10 mM DTT, 0.1 mM NaN_3, pH 6.90 at 30 °C.

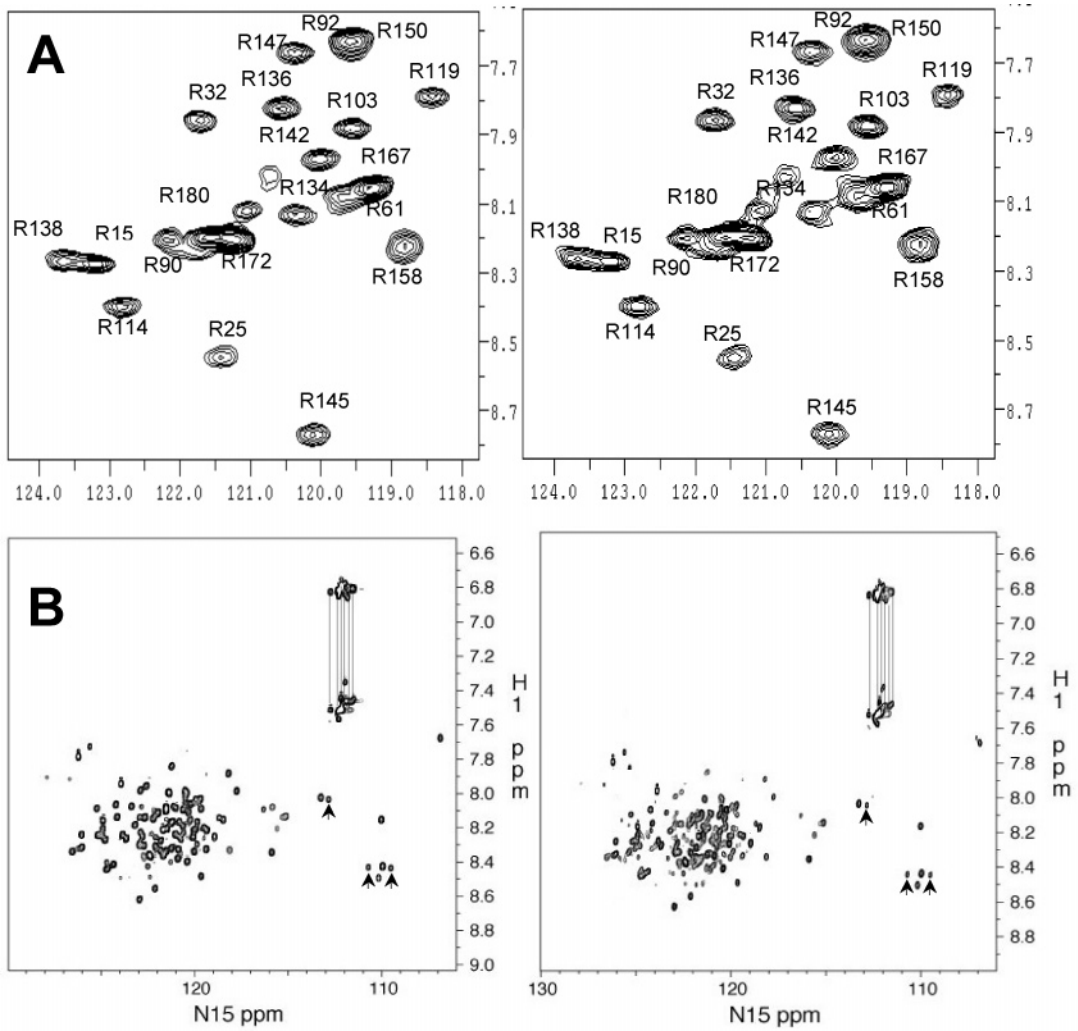

FIGURE 8: Panel A: $^{1}H-^{15}N$ HSQC spectra of ^{15}N-Arg apoE3(1−183) without (left) and with 1:1 molar ratio of unlabeled apoE-J5(200−299) (right). The spectral assignment is based on our previous publication (*32*). Panel B: $^{1}H-^{15}N$ HSQC spectra of ^{15}N-labeled apoE-J5-(200−299) without (left) and with 1:1 molar ratio of unlabeled apoE3(1−199) (right). These NMR titration experiments were carried out at 30 °C.

residues. In panel B, we only observe 5−6 side chain cross-peaks of Gln and Asn; the rest are missing. This suggests that the missing side chain atoms of Gln and Asn are flexible and in fast exchange with D_2O. In contrast, in the context of full length of apoE3-J5, these side chain atoms are fixed and display much less flexibility, thus all of the side chain cross-peaks of Gln and Asn are observed.

The above results provide direct experimental evidence that apoE3 contains a weak domain−domain interaction that stabilizes the C-terminal domain. However, this weak domain−domain interaction does not seem to affect the structure of the N-terminal domain, since no major spectral differences were observed when the spectra of the N-terminal domain between full-length apoE3 and the isolated form were compared. The spectral difference of the apoE3(215−299)-J5 between an isolated domain and in the full-length protein suggests a possible conformational difference. Based on our NMR data, we suggest that this conformational difference is due to the reduction of the conformational flexibility of the C-terminal domain in the context of full-length apoE3, due to a weak domain−domain interaction. This suggestion is supported by two other pieces of spectral evidence. First, the conformational heterogeneity was absent in the C-terminal domain of the segmental-labeled, full-length apoE3, thus this domain only displays one set of signals. Second, the side chain atoms of Gln and Asn are fixed and become much less flexible in the context of full-length apoE3, displaying all of the cross-peaks of all Gln and Asn sidechains.

The Hinge Region (Residues 192−215) May Play a Critical Role in Mediating ApoE3's Domain−Domain Interaction. To identify the structural basis of the domain−domain interaction, we performed NMR titration experiments. Figure 8, panel A, shows $^{1}H-^{15}N$ HSQC spectra of ^{15}N-Arg labeled apoE3(1−183) without (left) and with unlabeled apoE(200−299)-J5 (right) at a 1:1 molar ratio. Since apoE(200−299)-J5 is unlabeled, it does not display signals in this spectrum. No spectral difference is observed between the two spectra, indicating the absence of domain interaction when the two domains are present as fragments. The same result is also found when we titrated both unlabeled apoE3(1−199) to labeled apoE(200−299)-J5 (Figure 8, Panel B) and unlabeled apoE3(1−214) to labeled apoE(215−299)-J5 (data not shown). We also carried out NMR titration of unlabeled apoE(1−183) to labeled apoE(215−299)-J5 and observed no spectral changes after titration (data

not shown). In this case, the hinge region between the N- and C-terminal domains (residues 184−214) is missing during the titration.

The identical spectra of an isolated C-terminal domain with and without an isolated N-terminal domain fragment in all three cases indicate that there is no domain−domain interaction when the two isolated domain fragments are present. This conclusion is confirmed by a comparison of Figures 7 and 8, since the specific spectral differences shown in Figure 7 were not observed in Figure 8, panel B. For example, the conformational heterogeneity of two Gly residues is retained after titration with an isolated apoE N-terminal domain (arrows, panel B, Figure 8). In addition, the side chain atoms of Gln and Asn remain flexible after titration of apoE N-terminal domain, since only 5−6 side chain NH_2 of Gln and Asn are observed (dotted lines, panel B, Figure 8). Thus, an isolated apoE C-terminal domain retains conformational heterogeneity and flexibility, even in the presence of an isolated apoE N-terminal domain fragment with or without the hinge region (apoE3(1−214) or (apoE3(1−183)). This is in sharp contrast to the C-terminal domain spectrum in the full-length apoE (Figure 7, right panel), indicating that the hinge region is required to maintain the tertiary structure of the apoE C-terminal domain, likely acting as a tether to position the two domains in close contact for the weak interaction that stabilizes the structure of the C-terminal domain in full-length apoE. Previously, using the FRET technique, Narayanaswami and co-workers also suggested that this hinge region in apoE3 might be critical to maintain the define orientation of the two apoE domains (*35*).

ACKNOWLEDGMENT

The authors would like to thank Dr. David Waugh for his generosity for providing us with the auxotrophic bacterial strains for specific labeling of the apoE N-terminal domain. The authors also thank Ms. Victoria Meiners for critical reading the manuscript.

REFERENCES

1. Weisgraber, K. H. (1994) Apolipoprotein E: structure-function relationships, *Adv. Protein Chem. 45*, 249−302.
2. Mahley, R. W., and Rall, S. C., Jr. (2000) Apolipoprotein E: far more than a lipid transport protein, *Annu. Rev. Genomics Hum. Genet. 1*, 507−537.
3. Mahley, R. W. (1988) Apolipoprotein E: cholesterol transport protein with expanding role in cell biology, *Science 240*, 622−630.
4. Huang, Y., von Eckardstein, A., Wu, S., Maeda, N., and Assmann, G. (1994) A plasma lipoprotein containing only apolipoprotein E and with gamma mobility on electrophoresis releases cholesterol from cells, *Proc. Natl. Acad. Sci. U.S.A. 91*, 1834−1838.
5. Mahley, R. W., and Huang, Y. (1999) Apolipoprotein E: from atherosclerosis to Alzheimer's disease and beyond, *Curr. Opin. Lipidol. 10*, 207−217.
6. Zannis, V. I., Breslow, J. L., Utermann, G., Mahley, R. W., and Weisgraber, K. H. (1982) Proposed nomenclature of apoE isoproteins, apoE genotypes, and phenotypes, *J. Lipid Res. 23*, 911−914.
7. Rall, S. C., Jr., Weisgraber, K. H., and Mahley, R. W. (1982) Human apolipoprotein E. The complete amino acid sequence, *J. Biol. Chem. 257*, 4171−4178.
8. Schneider, W. J., Kovanen, P. T., Brown, M. S., Goldstein, J. L., and Utermann, G. (1981) Familial dysbetalipoproteinemia. Abnormal binding of mutant apoprotein E to low density lipoprotein receptors of human fibroblasts and membranes from liver and adrenal of rats, rabbits, and cows, *J. Clin. Invest. 68*, 1075−1085.
9. Weisgraber, K. H., Innerarity, T. L., and Mahley, R. W. (1982) Abnormal lipoprotein receptor-binding activity of the human E apoprotein due to cysteine-arginine interchange at a single site, *J. Biol. Chem. 257*, 2518−2521.
10. Luc, G., Bard, J. M., and Arreiler, D., et al. (1994) Impact of apolipoprotein E polymorphism on lipoproteins and risk of myocardial infarction. The ECTIM Study, *Arterioscler. Thromb. 14*, 1412−1419.
11. Weisgraber, K. H., and Mahley, R. W. (1996) Human apolipoprotein E: the Alzheimer's disease connection, *FASEB J. 10*, 1485−1494.
12. Corder, E. H., Saunders, A. M., Strittmatter, W. J., Schmechel, D. E., and Gaskell, P. C. (1993) Gene dose of apolipoprotein E type 4 allele and the risk of Alzheimer's disease in late onset families, *Science 261*, 921−923.
13. Saunders, A. M., Strittmatter, W. J., and Schmechel, D. et al. (1993) Association of apolipoprotein E allele epsilon 4 with late-onset familial and sporadic Alzheimer's disease, *Neurology 43*, 1467−1472.
14. Wilson, C., Wardell, M. R., Weisgraber, K. H., Mahley, R. W., and Agard, D. A. (1991) Three-dimensional structure of the LDL receptor-binding domain of human apolipoprotein E, *Science 252*, 1817−1822.
15. Peters-Libeu, C. A., Newhouse, Y., Hatters, D. M., and Weisgraber, K. H. (2006) Model of biologically active apolipoprotein E bound to dipalmitoylphosphatidylcholine, *J. Biol. Chem. 281*, 1073−1079.
16. Dong, L-M, Wilson, C., Wardall, M. R., Simmons, T., and Mahley R. W. (1994) Human apolipoprotein E. Role of arginine 61 in mediating the lipoprotein preferences of the E3 and E4 isoforms, *J. Biol. Chem. 269*, 22358−22365.
17. Dong, L.-M., Parkin, S., Trakhanov, S. D., Rupp, B., and Simmons, T., et al. (1996) Novel mechanism for defective receptor binding of apolipoprotein E2 in type III hyperlipoproteinemia, *Nat. Struct. Biol. 3*, 718−722.
18. Dong, L.-M., and Weisgraber, K. H. (1996) Human apolipoprotein E4 domain interaction. Arginine 61 and glutamic acid 255 interact to direct the preference for very low density lipoproteins, *J. Biol. Chem. 271*, 19053−19057.
19. Hatters, D. M., Peters-Libeu, C. A., and Weisgraber, K. H. (2006) Apolipoprotein E structure: insights into function, *Trends Biochem. Sci. 31*, 445−454.
20. Mahley, R. W., Weisgraber, K. H., and Huang, Y. (2006) Apolipoprotein E4: a causative factor and therapeutic target in neuropathology, including Alzheimer's disease, *Proc. Natl. Acad. Sci. U.S.A. 103*, 5644−5651.
21. Hatters, D. M., Budamagunta, M. S., Voss, J. C., and Weisgraber, K. H. (2005) Modulation of apolipoprotein E structure by domain interaction: differences in lipid-bound and lipid-free forms, *J. Biol. Chem. 280*, 34288−34295.
22. Fan, D., Li, Q., Korando, L., Jerome, W. G., and Wang, J. (2004) A monomeric human apolipoprotein E carboxyl-terminal domain, *Biochemistry 43*, 5055−5064.
23. Waugh, D. S. (1996) Genetic tools for selective labeling of proteins with alpha-15N-amino acids, *J. Biomol. NMR 8*, 184−192.
24. MacDonald, R. C., MacDonald, R. I., Menco, B. Ph. M. Takeshita, K., Subbarao, N. K., and Hu, L. (1991) Small-volume extrusion apparatus for preparation of large, unilamellar vesicles, *Biochim. Biophys. Acta 1061*, 297−303.
25. Surewicz, W., Epand, R. M., Pownall, H. J., and Hiu, S.-K. (1986) Human apolipoprotein A-I forms thermally stable complexes with anionic but not with zwitterionic phospholipids, *J. Biol. Chem. 261*, 16191−16197.
26. Jonas, A. (1986) Reconstitution of high-density lipoproteins, *Methods Enzymol. 128*, 553−582.
27. Jonas, A., Kezdy, K. E., and Wald, J. H. (1989) Defined apolipoprotein A-I conformations in reconstituted high density lipoprotein discs, *J. Biol. Chem. 264*, 4818−4824.
28. Innerarity, T. L., Friedlander, E. J., Rall, S. C., Jr., Weisgraber, K. H., and Mahley, R. W. (1983) The receptor-binding domain of human apolipoprotein E. Binding of apolipoprotein E fragments, *J. Biol. Chem. 258*, 12341−12347.
29. Pace, C. N., Shirley, B. A., and Thomson, J. A. (1989). in *Protein Structure and Function: a practical approach* (Creighton, T. E., Ed.) LRL Press, Oxford.

30. Delaglio, F., Grzesiek, S., Vuister, G. W., Zhu, G., Pfeifer, J., and Bax, A. (1995) NMRPipe: a multidimensional spectral processing system based on UNIX pipes, *J. Biomol. NMR 6*, 277−293.
31. Ren, X., Zhao, L., Sivashanmugam, A., Miao, Y., Korando, L., Yang, Z., Reardon, C. A., Getz, G. S., Brouillette, C. G., Jerome, W. G., and Wang, J. (2005) Engineering mouse apolipoprotein A-I into a monomeric, active protein useful for structural determination, *Biochemistry 44*, 14907−14919.
32. Xu, C., Sivashanmugam, A., Hoyt, D., and Wang, J (2005) A complete backbone assignment of the apolipoprotein E LDL receptor binding domain, *J. Biomol. NMR. 32*, 177.
33. Wetterau, J. R., Aggerbeck, L. P., Rall, S. C., Jr., and Weisgraber, K. H. (1988) Human apolipoprotein E3 in aqueous solution. I. Evidence for two structural domains, *J. Biol. Chem. 263*, 6240−6248.
34. Roheim, P. S., Carey, M., Forte, T., and Vega, G. L. (1979) Apolipoproteins in human cerebrospinal fluid, *Proc. Natl. Acad. Sci. U.S.A. 76*, 4646−4649.
35. Narayanaswami, V., Szeto, S. S., and Ryan, R. O. (2001). Lipid association-induced N- and C-terminal domain reorganization in human apolipoprotein E3, *J. Biol. Chem. 276*, 37853−37860.
36. Morrow, J. A., Segall, M. L., Lund-Katz, S., Phillips, M. C., Knapp, M., Rupp, B., and Weisgraber, K. H. (2000). Differences in stability among the human apolipoprotein E isoforms determined by the amino-terminal domain, *Biochemistry 39*, 11657−11666.

BI700672V